

SASsy sonar



Alden Denny

Denny, Hansen, Sæbø and Pedersen tackle the challenge of using acoustic remote sensing to map seafloor mineral deposits in the deep ocean.

Who should read this paper?

This paper should be read by anyone with an interest in deep ocean exploration.

Why is it important?

Highly detailed remote sensing of the Earth from space is now almost routine. The same may not be said for the deep ocean. Synthetic aperture sonar (SAS), the doppelganger of synthetic aperture radar, holds promise of high resolution remote sensing of the deep ocean, but the merits of this technology remain largely unproven.



Roy Edgar Hansen

One very practical application for deep ocean mapping technology is the delineation of seafloor massive sulfide deposits generated by hydrothermal systems at plate tectonic spreading centres. In this paper the authors evaluate the pros and cons of using synthetic aperture sonar mounted on an autonomous underwater vehicle as a tool for mapping such deposits. Based on a trial survey in the area of the Arctic Mid-Ocean Ridge, they conclude that the fine resolution and large areal coverage possible with SAS enables highly efficient mapping of the seabed with a resolution sufficient to determine the location of active and extinct hydrothermal systems. Furthermore, the authors point out that the high-resolution SAS data could also be used for post-extraction impact assessment. Steep terrain and significant thermal discontinuities associated with active hydrothermal vents can lead to artifacts in the SAS data, but these challenges are endemic to any imaging sonar system.



Torstein Olsmo Sæbø

Synthetic aperture sonar technology is currently commercially available from multiple vendors including Kongsberg Maritime, Kraken Sonar Systems and Raytheon.



Rolf B. Pedersen

About the authors

Alden Denny is a doctoral student at the University of Bergen, where he is exploring the application of advanced remote sensing techniques to marine geology. His specialty is the exploration and characterization of seafloor hydrothermal systems. He works with a wide variety of techniques including multibeam and single beam echo sounders, synthetic aperture sonar, magnetometry, and gravimetry. Roy Edgar Hansen holds M.Sc. and PhD degrees in physics from the University of Tromsø. He is currently the principal scientist and project manager for autonomous underwater vehicle and synthetic aperture sonar development at the Norwegian Defence Research Establishment (FFI), and is an adjunct associated professor with the Department of Informatics at the University of Oslo. Torstein Olsmo Sæbø holds B.Sc. and M.Sc. degrees in astrophysics from the University of Oslo and a PhD from the University of Tromsø. He is a senior scientist at FFI, specializing in the field of interferometric synthetic aperture sonar. Rolf B. Pedersen holds a PhD in geology from the University of Bergen. He is currently the director of the Centre for Geobiology, a Centre of Excellence focusing on deep sea research and geo-biological interactions. A central theme of his research is the deep sea and the formation of oceanic lithosphere.

THE USE OF SYNTHETIC APERTURE SONAR TO SURVEY SEAFLOOR MASSIVE SULFIDE DEPOSITS

Alden Ross Denny¹, Torstein Olsmo Sæbø², Roy Edgar Hansen², and Rolf Birger Pedersen¹

¹University of Bergen Centre for Geobiology, Bergen, Norway

²Norwegian Defence Research Establishment (FFI), Kjeller, Norway

ABSTRACT

With the advent of advanced deep sea mining technology, seafloor mining is poised to begin on a global scale. For the success of any mining operation, it is crucial that both the operators and regulatory bodies possess detailed information of the resource and surrounding environment during all stages of the mining process. We propose that synthetic aperture sonar (SAS) is a key emerging technology that can be used by all relevant parties at only a minimal increase in cost. This technology, originally designed for military and offshore oil and gas industry applications, can be readily applied to scientific seafloor mapping. The fine resolution of this technique allows for deposit mapping of active and inactive seafloor massive sulfide deposits. By clearly distinguishing between volcanic and hydrothermal landscapes based on features finer than the resolution of conventional multibeam systems, SAS enables an entirely new level of hydrothermal deposit survey.

This technology was employed during a detailed survey of shallow hydrothermal systems on the Arctic Mid-Ocean Ridge system. Here we present preliminary results from a newly discovered venting area adjacent to the Troll Wall field, southern Mohns Ridge. This area has extensive high and low temperature hydrothermal accumulations with variable surface morphology, which appear in SAS imagery to be distinct from adjacent volcanic and tectonic structures. SAS images, when coupled with assays from ROV rock samples, will enable rapid deposit estimation for this novel Arctic hydrothermal mineral resource.

KEYWORDS

Seafloor survey; Marine mining; SAS; Seafloor massive sulfides; Hydrothermal vents; Deposit mapping; Acoustic imaging

INTRODUCTION

Exploration and exploitation of marine mineral resources is a rapidly developing field energized by the increasing demand for base metals, the lack of new discoveries of economically viable on-land deposits, and the massive development of subsea technology for the oil and gas industry. Several nations have opened up to active extraction of seafloor mineral deposits within their respective exclusive economic zones (EEZ), with mining potentially beginning in early 2018 within the Papua New Guinea EEZ [Nautilus Minerals Inc., 2014]. Mineral exploration in international waters has been ongoing for the past 13 years with several leases for polymetallic nodules, maintained by the International Seabed Authority, due to begin extraction in early 2016 [Billett, 2014]. In shallow coastal water, marine mining for phosphate [Beavers, 2013] and precious stones [Heyes, 2002] has been ongoing for over 40 years. With the initiation of seafloor mining now imminent, both operators and regulatory agencies must develop detailed requirements for safe and environmentally responsible extraction. In this paper we propose that synthetic aperture sonar (SAS), as deployed on deep-dive autonomous underwater vehicle (AUV) platforms, can be a key tool for both operation and management organizations. Currently SAS systems are commercially available from multiple vendors; available systems include the Kraken Aquapix™, Kongsberg HISAS 1030, and Raytheon ProSAS 60. The Aquapix™ is a dual-frequency SAS with a swath width of ~600 m, which was recently used in the search for the *HMS Erebus*, a ship

from the lost Franklin expedition [Whiffen, 2014]. The Kongsberg HISAS 1030 has a 600 m swath width and a theoretical resolution of 3 x 3 cm, and is typically mobilized on the HUGIN AUV. The ProSAS 60 is a lower frequency SAS with an effective swath of 3,000 m and a theoretical resolution of 10 x 10 cm; this system is currently deployed as part of the flight MH370 search [The Economist, 2014]. In this study, all of the images have been created with the Kongsberg HISAS 1030 system, which was mobilized as the primary acoustic payload on the Norwegian Defense Research Establishment HUGIN AUV. With high resolution and large area coverage rate, SAS can potentially be an efficient tool for multiple purposes during the lifecycle of a marine mine including the initial site survey, extraction monitoring, and for post-extraction impact assessment.

METHODS

SAS Overview

Synthetic aperture sonar is based on the principle of collecting multiple pulse-echoes from sonars in side-looking geometry as illustrated in Figure 1 [Hansen, 2011]. The data collected are combined coherently to form a longer (synthetic) antenna such that the sonar angular (or along-track) resolution is improved. SAS is very similar to synthetic aperture radar (SAR) [Massonnet and Souyris, 2008]. Although the theoretical basis for SAS was first published in the mid-1980s [Hayes and Gough, 2009], SAS technology has only become readily available in the last few years. Today, SAS technology is accessible for use in various applications and available SAS systems can

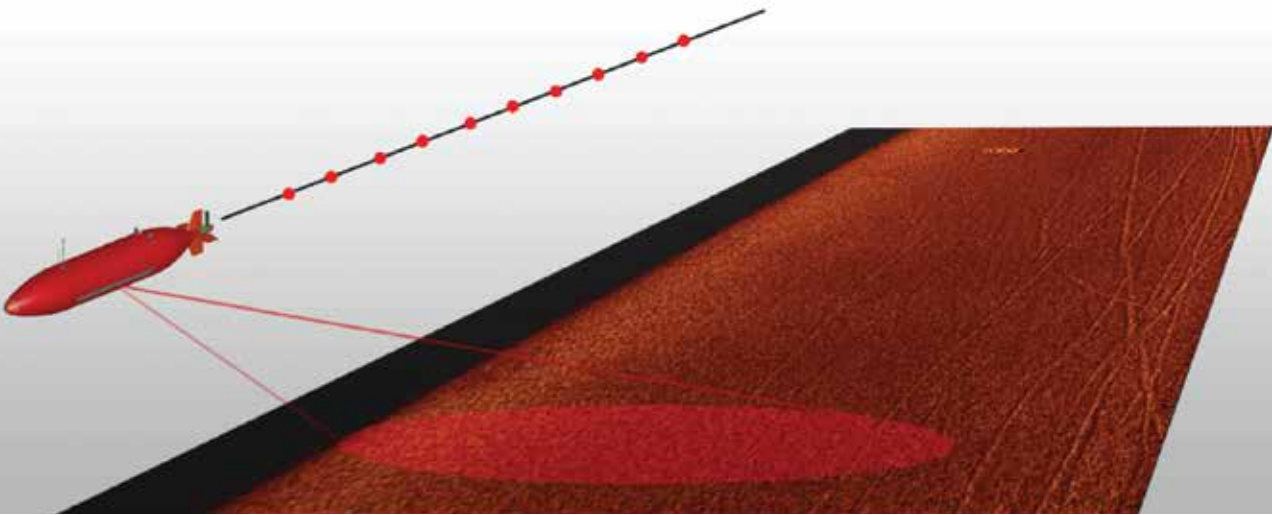


Figure 1: Principle of synthetic aperture sonar as applied on an AUV platform. The vehicle illuminates sequential overlapping regions which are then combined in post-processing to create a single sonar image.

provide resolution down to 2-3 cm and swath widths up to 1,500 m [Hansen, 2013].

Unlike other sonar technologies, SAS gives range-independent along-track resolution by increasing the aperture length as function of range. This provides a solution to a fundamental sonar problem of obtaining high angular resolution at long range. In traditional sonar (real aperture), higher resolution is obtained by increasing the acoustic frequency. This, inevitably, decreases the achievable range in the ocean: acoustic energy at higher frequencies is more readily absorbed [Lurton, 2010]. It is worth mentioning that although SAS image resolution becomes range independent, the image quality and the signal to noise ratio (SNR) in particular are still range dependent due to the transmission loss and other factors [Lurton, 2010].

Another benefit of SAS is that along-track resolution is independent of acoustic frequency for transmitter/receiver element-sizes larger than half a wavelength. This is achieved by increasing the length of the synthetic aperture when lowering the acoustic frequency. At the

lower limit, the classical (diffraction limited) resolution cannot be better than a quarter of a wavelength (in any dimension). The information content in the images will be frequency dependent. Noticeably, the angular spread increases with decreasing frequency – which again must lead to different information content in the images.

Data Processing

Figure 2 is a generalized flow chart for the data processing of SAS data. Auxiliary data such as navigational data about the track positions and sensor orientation, environmental data (the sound speed in particular), and the geometrical model for the imaging scene (the topography or bathymetry) must be known within an accuracy such that the SAS images can be constructed successfully [Cook, 2007]. This is non-trivial and imposes a strong requirement on the navigation system, which is generally not achievable even for advanced navigation systems on AUVs. Therefore most SAS systems (if not all) use some form of sonar data driven navigation correction (referred to as micronavigation) [Bellettini and Pinto, 2002]. A fundamental difference

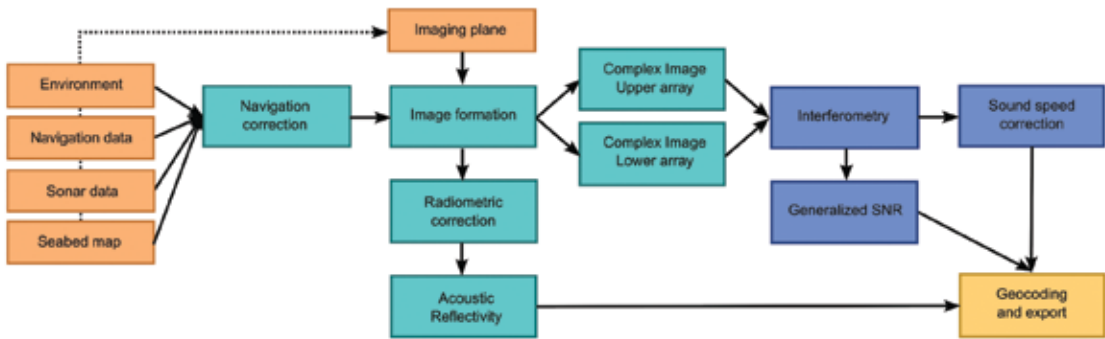


Figure 2: Synthetic aperture sonar processing flow including seabed depth estimation.

between SAR and SAS is that robustness in SAS is a major, and ongoing, topic [Hagen and Hansen, 2011; Hansen et al., 2011].

After the platform trajectory has been estimated and corrected, an imaging plane is chosen and a SAS image is formed by an imaging algorithm either in the time domain or the frequency domain [Hawkins, 1996; Massonnet and Souyris, 2008]. For interferometric SAS systems, such as the HISAS 1030, two images are constructed – one for the upper array and one for the lower array. These two images are constructed with a vertical baseline (a slightly different vertical look angle towards the seabed) such that the phase in the images contain information about the vertical direction towards each pixel in the imaging scene. Time difference of arrival processing can subsequently be applied such that the relative depth of the seabed in the imaging scene is estimated. This is referred to as interferometric processing, and is common in SAR [Hanssen, 2001; Jakowatz et al., 1996].

After a SAS image is constructed, its amplitude must be corrected to compensate for transmission loss and other effects [Lurton, 2010] so that the pixel values can be fully

utilized to estimate seabed parameters. Such processing is common in SAR where the estimated reflectivity is a very important parameter [Oliver and Quegan, 1998; Massonnet and Souyris, 2008]. Accurate correction requires, however, that the sonar hardware and software is absolutely calibrated. To our knowledge, no SAS (or side scan sonar) system is fully magnitude calibrated to date. This will be an important goal to achieve in future development of SAS systems [Lurton, 2010; Hansen, 2013].

SAS interferometry processing for seabed depth estimation contains a number of trade-offs and techniques. The vertical accuracy in the estimate is related to the range and the SNR [Hanssen, 2001], such that at longer range the standard deviation is always higher. All current interferometry techniques used in SAR and SAS use pixel averaging in the interferogram estimation, such that the seabed depth estimate always has poorer geometrical resolution than the image. This creates a trade-off between vertical accuracy and horizontal resolution. For marginal SNR cases and in large topographic variations, the seabed depth estimate from interferometry is susceptible to increased noise. A particular difficulty in

interferometry processing is the probability of estimating an incorrect wrap in the phase difference map, which leads to periodic errors in the estimated depth map. There are techniques to mitigate the errors by using signal bandwidth and specific advanced processing [Ghiglia and Pritt, 1998; Sæbø et al., 2013]. Finally, in the underwater domain sound speed variations cause acoustic refraction that must be compensated for, otherwise large-scale errors (bias) may occur in the seabed depth estimates [Lurton, 2010].

Deposit Mapping

Active Hydrothermal Systems

The challenge faced in mapping seafloor massive sulfide (SMS) deposits is in differentiating volcanic, tectonic, and hydrothermal morphologies to correctly assess the extent and depth of a mineralized zone. This typically requires direct imaging of the seafloor or a very high-resolution side scan survey, both of which are intensely time consuming (and consequently expensive) to collect.

To date a common SMS deposit mapping technique with AUV assets is done via a nested survey approach [Yoerger et al., 2007; German et al., 2008; Ferri et al., 2010]. The nested survey begins with a high-altitude multibeam mapping run, typically gridded at >2 m resolution and designed to give an overview of the area. On the mapping run, trackline data from the vehicle's CTD and nephelometer are used to identify any hydrothermal plume regions. Next, either through autonomous control [Yoerger et al., 2007] or on a subsequent deployment, the area covered is dramatically decreased: a lower vehicle altitude is used to create metre-

scale maps and detailed vehicle sensor grids, which culminate in a photomosaic survey of the prospective active venting site. This type of survey is excellent for locating SMS sites with active high-temperature venting in a reasonably small area, but is not optimal for assessing an area for potential mining activities. The nested survey design is unable to locate areas of extinct or diffuse venting, and only maps a region directly around an active hydrothermal vent at maximum resolution. For photomosaicked regions, structure-from-motion [Singh et al., 2007] can be used to create cm-resolution topographic renderings from image mosaics, but only for a relatively small-mosaicked region. For economic exploitation of seafloor mineral deposits, finding regions with multiple inactive vents is ideal [Lipton, 2012], a task that current survey techniques are ill suited to accomplish.

SAS has the potential to solve some of the survey issues described above by surveying large areas at fine resolution. The SAS imagery can then be used to differentiate the surficial geology of the entire survey region. At SAS-achievable resolutions, it should be possible to differentiate between volcanic, tectonic, and hydrothermal morphologies. This means that active venting systems can be identified by the morphology of the venting edifice, independent of the dispersion of the hydrothermal plume; a notoriously fickle indicator in the search for hydrothermal systems [Veirs et al., 1999].

Extinct Hydrothermal Systems

Current techniques for mapping extinct hydrothermal systems focus on the large-scale

spreading ridge morphology from ship-based multibeam [Devey et al., 2013] and on the magnetic signal generated from hydrothermal flow. In basalt-hosted hydrothermal systems, the flow of hydrothermal fluid alters magnetic minerals in the basalt, causing de-magnetized regions corresponding to areas of fluid flow [Tivey and Johnson, 2002; Szitkar et al., 2014A]. In ultramafic-hosted hydrothermal systems, hot fluid flow causes the precipitation of magnetic minerals and consequently creates a magnetic high in the otherwise un-magnetic ultramafic substrate [Szitkar et al., 2014B]. The magnetic signature of hydrothermal systems is a key tool in locating extinct venting systems that lack a distinct surface expression due to erosion of the friable hydrothermal chimneys and persistent (though typically slow) pelagic sedimentation [Tivey et al., 2014]. The drawback to magnetics data is that it does not provide information as to the degree or type of mineralization present, but rather is merely an indicator of past hydrothermal flow. Consequently, magnetics can be used to locate regions of past or present hydrothermal activity, but cannot inform on the type of deposit or economic viability of the region. However, magnetics data is reasonably simple to collect as the magnetometer is typically deployed in the mapping vehicle and collects data during a standard bathymetric survey mission, rendering this technique an ideal add-on to existing survey missions.

A combination of SAS and magnetometer survey is also ideal for identifying extinct hydrothermal systems with sediment cover. In typical marine environments, sediment cover of 0.5 to 1 m is sufficient to mask the key topographic features used to distinguish

hydrothermal morphologies from adjacent volcanic and tectonic morphologies. For example, a conical pile of basalt pillows is morphologically distinct from a hydrothermal chimney, but only when the critical slope and pillow morphology are exposed. Sediment cover blocking those key features would render the observer unable to distinguish between the two deposit types, though low-frequency SAS may provide enough sediment-cover penetration to alleviate this issue. In young oceanic crust (<5 mya), sedimentation is largely controlled by re-suspension of pelagic sediment in the nepheloid layer [Mitchell et al., 1998]. Consequently, sediment distribution is largely dependent on the formation of basins rather than on the age of the oceanic crust. For exploration purposes this means that accurate identification of the surficial morphology of an area is key in interpreting the magnetic signal, as the sediment cover will attenuate the magnetic signal. Co-registration of the magnetic data with SAS imagery could remove some ambiguity in the magnetics data due to sediment cover: visual interpretation of the SAS imagery can provide an estimate of the sediment layer thickness. It should be noted that broadband SAS including low frequencies and high frequencies might give additional information about the sub-sediment texture [Sternlicht et al., 2012].

EXAMPLE SITE: SOUTHERN MOHNS RIDGE

The Arctic Mid-Ocean Ridge (AMOR) system is a collection of ultra-slow spreading ridges extending from the Icelandic hotspot to the far north [Pedersen et al., 2010B]. Within the



Figure 3: Jan Mayen Island hotspot and surrounding mid-ocean ridges. Both the northern Kolbeinsey Ridge (left) and southern Mohns Ridge (right) are highly elevated with respect to the rest of the Arctic Mid-Ocean Ridge (AMOR) system. This elevation is due to the combination of a slow spreading rate and increased magmatic input from the Jan Mayen hotspot (Pedersen et al., 2010A). The red box highlights the area covered in Figure 4, which is the southern-most spreading segment of the Mohns Ridge.

AMOR the northern Kolbeinsey Ridge and Mohns Ridge (Figure 3) both lie within the ice-free Norwegian EEZ, and are of interest for marine mineral exploration [Ellefmo, 2014]. The first systematic exploration of the AMOR for the presence of hydrothermal systems began in 2001 as part of the SUBMAR program, and at least four systems have since been discovered [Pedersen et al., 2005; Pedersen et al., 2009; Pedersen et al., 2010B; Baumberger et al., 2013]. One area of particular interest is the intersection of the AMOR with the Jan Mayen hotspot, which has contributed to prolific volcanism along the northern Kolbeinsey Ridge and southern orthogonally spreading Mohns Ridge (Figure 3). The southern Mohns Ridge rises to a shoal depth of 420 m depth, as compared to the average depth of ~2,300 m depth for spreading centres on the rest of the Mohns Ridge. The abnormally shallow depth made this location

an early target in the search for hydrothermal systems, and in 2005 Pedersen et al. located the Troll Wall hydrothermal system.

The Troll Wall system is situated on the eastern flank of the active rifted spreading centre. Since its discovery, this location has been acoustically mapped from hull mounted systems in 2008, 2011, 2012, and 2014, with repeat surveys over the venting systems and successive expansion of the surveyed area. In 2013 two additional active vent sites were discovered on the eastern flank of the segment, both at junctions of major N-S trending normal faults.

RESULTS

With the location of the two new vent fields discovered during the 2013 survey, in 2014 the Centre for Geobiology at University of Bergen

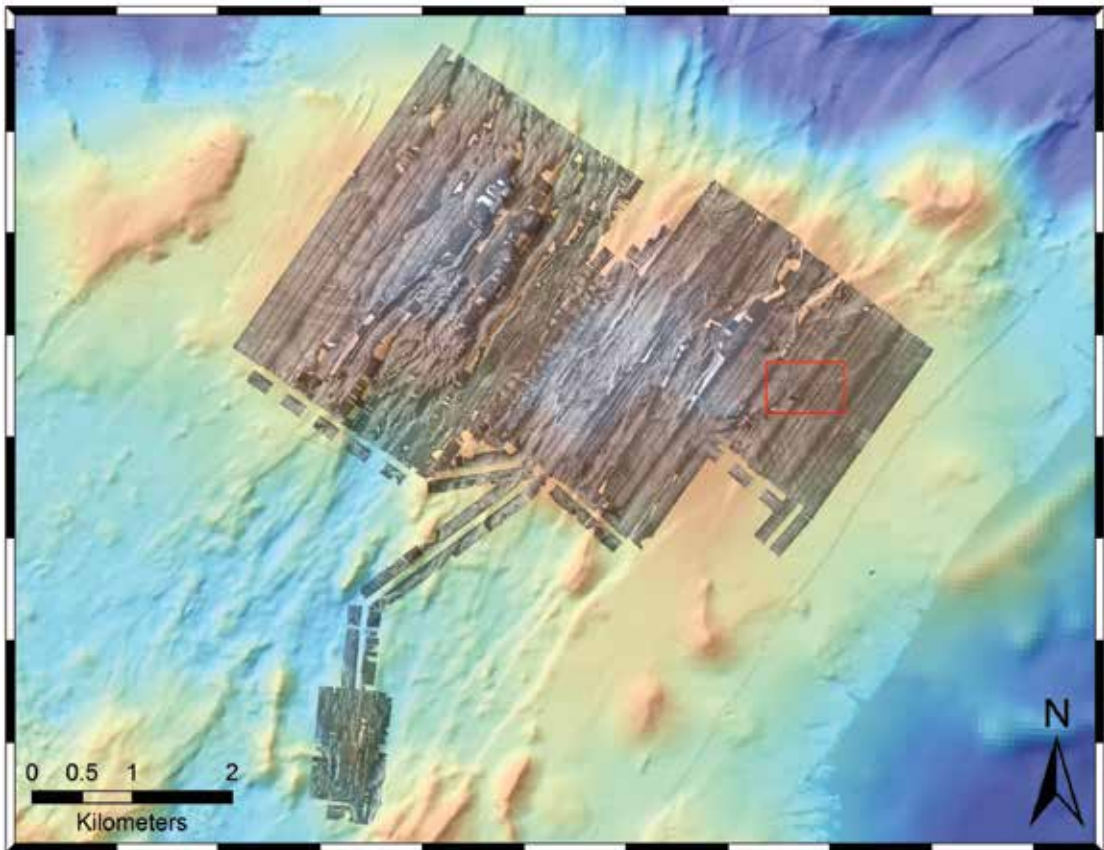


Figure 4: Shaded relief bathymetry of the southern Mohns Ridge orthogonal spreading centre overlain with the 2014 HISAS coverage collected by the HUGIN AUV. The red inset box delineates the area covered in Figure 5.

used the HUGIN AUV equipped with the HISAS 1030 SAS system to image both hydrothermal sites and the surrounding seafloor. The HUGIN AUV imaged ~ 21 km², including the central rift valley and both flanks of the spreading centre (Figure 4). The SAS data was collected in three dives, each under eight hours in duration. The special focus of this deployment was on the flanks of the volcano after the 2013 discovery of off-axis venting on the eastern flank of the spreading centre. The SAS investigation clearly identified the two new hydrothermal vents on the eastern flank, and did not locate any additional sites of focused hydrothermal venting on the western flank. On the eastern flank, the SAS imaging area covered the newly

discovered vent fields (Figure 5). Detailed images of several locations of interest were produced to illustrate the different volcanic, tectonic, and hydrothermal morphologies contained in the SAS image and interferometric bathymetry. Where possible, each SAS image is paired with an ROV video capture of the seafloor in that region to illustrate the accuracy of the SAS acoustic image product. The SAS images are formed using the back projection algorithm. Seabed depth is estimated using the complex cross correlation technique for wideband interferometry [Sæbø et al., 2013]. The SAS images have a theoretical single look complex resolution of approximately 3 x 3 cm, and the geometrical resolution in the seabed depth



Figure 5: Overview of two new hydrothermal deposits discovered through multibeam sonar maps in 2013 and directly imaged during the summer of 2014. The vents, marked by red boxes, are visible by the mounds of hydrothermal debris and “flares” of hot water distorting the acoustic image.

estimates is 18 x 18 cm. The SAS images are despeckled using a multitaper despeckling technique [Austeng et al., 2013], resulting in SAS images with reduced variance and a geometrical resolution of around 9 x 9 cm.

Figure 6 illustrates the end-member of diffuse venting hydrothermal flow, which develops as extensive microbially mediated iron-oxide ridges and nodule-like deposits [Thorseth et al., 2007; Øvreås et al., 2007]. These features are ubiquitous within 1 to 2 km of a hydrothermal system (Figure 5, centre), and represent regions of extensive low-temperature iron-oxide mineralization that is heavily constrained by near-surface faulting. These diffuse flow systems are well imaged using

SAS, as the fluid flow is far too low temperature to interfere with the image formation. Focused flow deposits (Figures 5 and 7) proved to be more challenging, as the assumed sound velocity profile is wildly inaccurate in the presence of >250°C jets of hydrothermal fluid.

Figure 7 is a SAS image of an actively venting hydrothermal system that lies on the outskirts of one of the vigorously venting hydrothermal fields. The SAS image of this formation suffers from only slight defocusing seen surrounding the shadow region of the vent, largely due to the relatively low temperature of the vent fluid as compared the adjacent >250°C vent systems (right-hand box, Figure

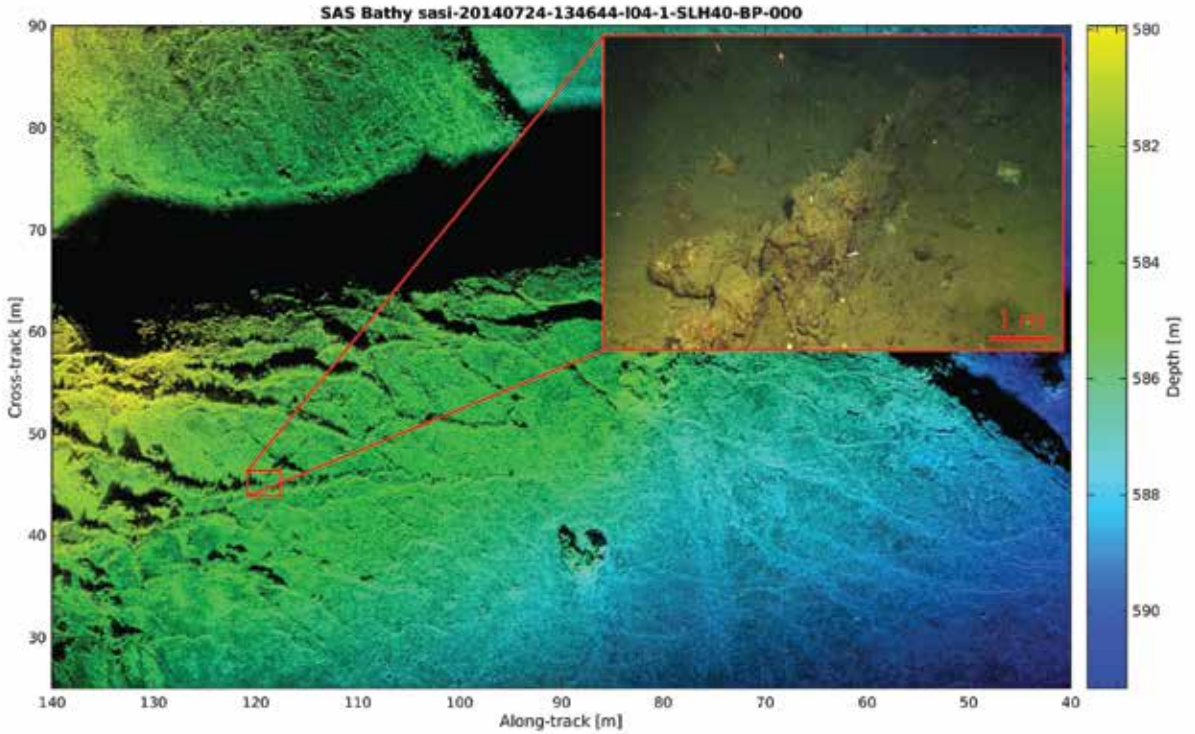


Figure 6: Comparison of full-resolution SAS imagery to direct ROV video capture of low-temperature iron-oxide hydrothermal deposit. In the SAS image, 20-50 m long ridges are visible in the left of the image. These ridges were seen imaged directly during a deployment of the ROV Aglantha (inset image). The elongate iron-oxide ridges are thought to grow along faulted diffuse flow pathways. These represent the alteration and degradation of an SMS deposit due to oxidation at near-ambient conditions.

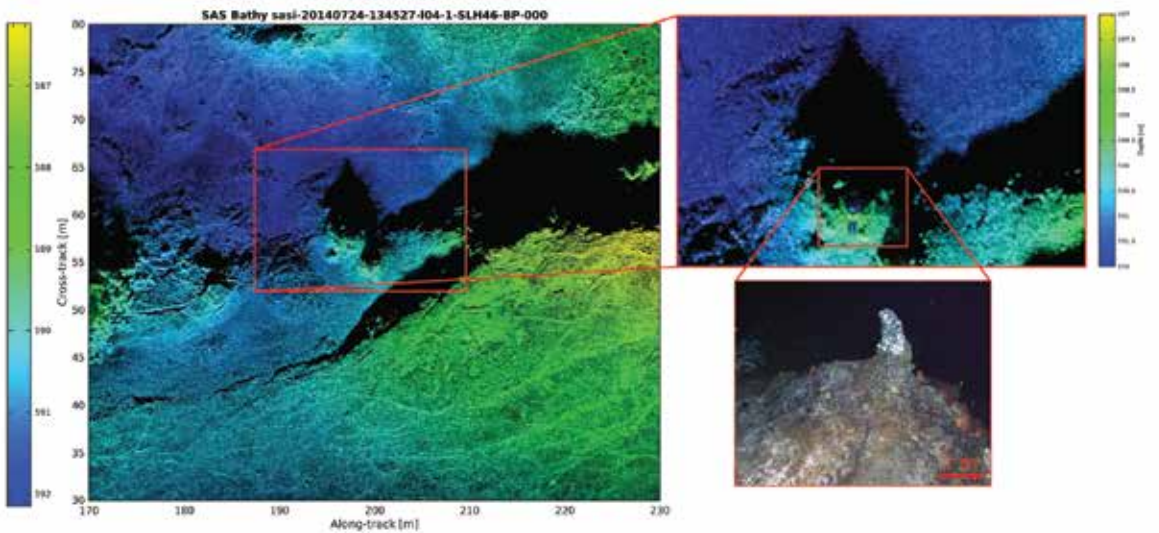


Figure 7: Comparison of a SAS fusion image to direct ROV imagery of a low-flow hydrothermal feature. Diffuse flow structures are comparatively easy to image, as the thermal gradient does not substantially degrade the sonar image. Note that the wide blanket of hydrothermal debris is well-imaged, whereas the actively venting summit is only seen by its shadow profile.

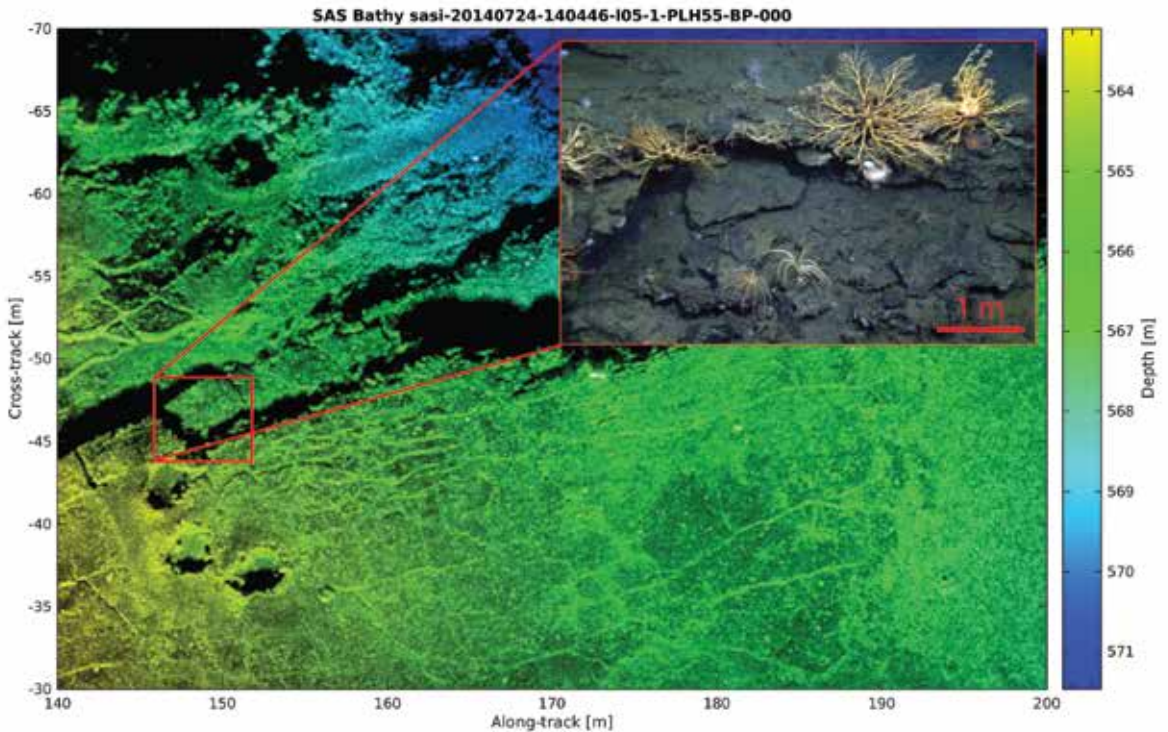


Figure 8: Comparison of SAS sonar image to direct ROV imagery of a faulted offset in partially hydrothermally altered sediment. Note the largely rectangular fracture patterns and faulted offsets typical of recent tectonic activity.

5). The SAS image of the venting structure contains a phase-wrapping error, seen on both the near and far sides of the vent as blocks of blue surrounded by green. This type of error is intrinsic in the use of an interferometric system in regions where the local topographic variation is near to or larger than the wrapping distance. In comparison to the submersible video still (Figure 7 inset), it is clear that the SAS image accurately depicts the sizeable pile of talus that surrounds this hydrothermal chimney: the extent of a hydrothermal mound is a key element to making deposit estimates. While the detailed imaging of the actively venting summit is challenging given the high-temperature fluid flow, the spatial extent of the formation is captured well in the SAS image.

Tectonically dominated terrain (Figure 8) is a difficult environment for stable vehicle flight:

rapidly changing seafloor topography makes it challenging to fly a level profile with respect to the topography. In this case, careful selection of the dive tracklines running parallel to the strike of major faults resulted in excellent imaging of the fault faces. While the main examples of hydrothermal flow do co-occur with faults in many hydrothermal environments, the main challenge presented by this terrain is in mission planning. The detailed SAS sonar image and bathymetry product clearly show the differences in faulted versus hydrothermal terrain. The tendency of hydrothermal systems to create either networks of interconnected ridges (Figure 6) that lack block rotation or in forming conical talus deposits surrounding a central spire (Figure 7) mean that a skilled observer can distinguish between these different morphologies and the adjacent tectonic features. Automated seabed

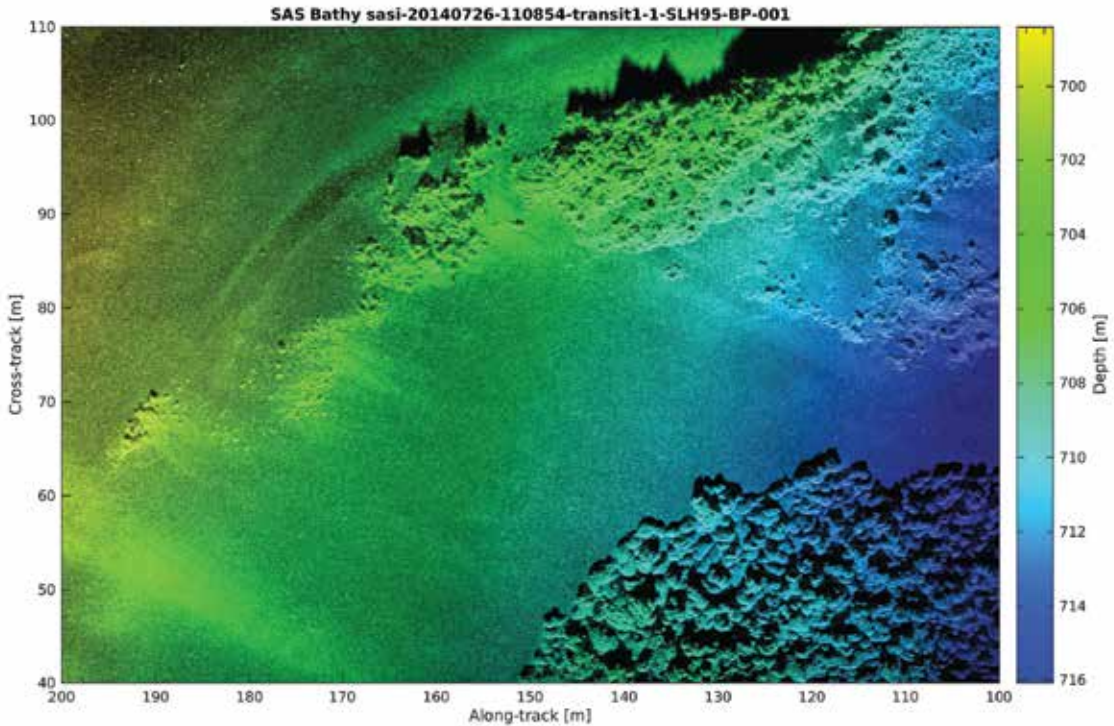


Figure 9: This is a SAS fusion image of the termination of a recent lava flow with pillow texture (lower right) in contrast to the underlying sediment and older flow ridge in the upper right of the image.

segmentation [Cobb and Principe, 2011; Cobb et al., 2010] may be a potential technique to apply in this type of SAS image interpretation.

Seafloor volcanic textures were not imaged with an ROV during the 2014 expedition, but were imaged in the SAS survey (Figure 9). Fresh and altered volcanic facies commonly underlie hydrothermal systems; the same magma chamber that supplies the heat for hydrothermal circulation also erupts as lavas on the seafloor. In this image, there is a clear distinction between fresh pillow basalts and an older volcanic ridge. Distinguishing between various generations of volcanic activity is critically important when studying seafloor volcanoes. The volume of magma release in each eruptive event is a highly informative parameter for understanding the dynamics of a volcanic complex [Caress et al., 2012].

Individual lava flows have varying morphology [Fundis et al., 2010] making the eruptive volume from individual events a poorly constrained parameter in seafloor volcanological studies. Regions of recent volcanism are primary targets when searching for seafloor hydrothermal systems, though seafloor volcanism can also destroy the surface expression of even large hydrothermal deposits.

DISCUSSION

Synthetic aperture sonar has the potential to transform the process of surveying for seafloor mineral deposits. The fine resolution and large areal coverage possible with SAS allows for the surficial geology of a prospective area to be investigated in one survey operation. This level of resolution does come with some limitations. SAS processing is a

computationally intensive process, which makes the creation of full-resolution SAS mosaics cumbersome. Current workflows involve creating a lower resolution overview mosaic to locate regions of interest and subsequent creation of detailed images of specific features. This workflow is largely successful, but the creation of a full-resolution, tiled, and scalable mosaic of a survey area would fully enable the geologic interpretation of a deposit area.

Another complication is that the presence of hydrothermal fluid causes a de-focusing of the acoustic image, severely degrading the image directly over vigorously venting systems. This error is inherent in any acoustic system, as the presence of hydrothermal fluid flow invalidates the assumed sound velocity profile, but it is especially evident in SAS images given the large number of pings that are combined in a single synthetic aperture. Additionally, rough terrain that cannot be compensated for with a variation in the imaging plane will defocus the SAS image and allow potential wrapping errors in the interferometric bathymetry product. These errors are unfortunately prevalent in active hydrothermal systems, as they are frequently hosted on steep fault scarps [Kelley et al., 2005; Kelley and Shank, 2010; Krasnov et al., 1995]. These types of errors are less prevalent at recently extinct or diffuse venting sites – the type of deposit that is more favourable to economic exploitation [Lipton, 2012].

The application of SAS to marine geological exploration will require further work in improving SAS performance in geologically complex terrain. While the HISAS 1030

system performed admirably well in and around the Jan Mayen vent sites, numerous locations suffered from poor image formation due to complex vehicle motion caused by erratic terrain. Improvement in the vehicle's terrain-following ability and platform stability, coupled with the application of more advanced SAS imaging geometries, would greatly improve the overall system performance.

CONCLUSION

Management of marine mineral extraction will require a regional understanding of the marine environment at a resolution that is relevant to both the extraction process and the impact of that extraction [Boschen et al., 2013]. The SAS images presented in this study (Figures 6 to 9) illustrate the utility of a fine-resolution system to differentiate between economically relevant geologic units by relying on a detailed view of the morphology and sonar image. SAS provides a tool to image large areas at fine resolution; this imaging is useful for the initial deposit estimation and seabed classification, which can be done rapidly over large survey areas with a minimal expenditure of vehicle time. For post-extraction impact assessment, repeat surveys using SAS could determine both the extent of extraction operations and the impact of the mining plume on the surrounding area. SAS is the only mature technology to provide fine-resolution imagery over large areas, which makes this tool ideal for exploration and management of marine mining operations.

ACKNOWLEDGMENT

We gratefully acknowledge the contributions of Ole Lorentzen and Eric Kleppe for their

superior work at sea on board the F/V *G.O.Sars*, and to Ana Filipa Marques and Emily Olesin for their review of this manuscript. We also acknowledge the anonymous reviewers for their insightful critiques of this paper, which have distinctly improved this manuscript. This work is funded from the Research Council of Norway through the Centre for Geobiology and from the EU 7th Framework through the MIDAS project.

REFERENCES

- Austeng, A.; Callow, H.J.; Larsen, Y.; and Hansen, R.E. [2013]. *Speckle reduction in synthetic aperture sonar images using Thomson's multitaper approach*. In proceedings of the 1st Underwater Acoustic Conference, Corfu, Greece, June.
- Baumberger, T.; Lilley, M.D.; Pedersen, R.B.; Thorseth, I.H.; and Stensland, A. [2013]. *Diverse hydrothermal venting at the Jan Mayen vent fields, AMOR*. Mineralogical magazine. Vol. 77, pp. 670.
- Beavers, C. [2013]. *An overview of phosphate mining and reclamation in Florida*. Masters dissertation, University of Florida.
- Bellettini, A. and Pinto, M.A. [2002]. *Theoretical accuracy of synthetic aperture sonar micromavigation using a displaced phase-center antenna*. IEEE Journal of Oceanic Engineering, Vol. 27, No. 4, pp. 780-789.
- Billett, M. [2014]. *An overview of the 2014 Stakeholder Survey by the ISA*. Presentation to the MIDAS-EU project meeting, Azores, Portugal.
- Boschen, R.E.; Rowden, A.A.; Clark, M.R.; and Gardner, J.P.A [2013]. *Mining of deep-sea seafloor massive sulfides: A review of the deposits, their benthic communities, impacts from mining, regulatory frameworks and management strategies*. Journal of Ocean and Coastal Management, Vol. 84, pp. 54-67. doi:10.1016/j.ocecoaman.2013.07.005.
- Caress, D.W.; Clague, D.A.; Paduan, J.B.; Martin, J.F.; Dreyer, B.M.; Chadwick, W.W.; Denny, A.; and Kelley, D.S. [2012]. *Repeat bathymetric surveys at 1-metre resolution of lava flows erupted at Axial Seamount in April 2011*. Nature Geosciences Vol. 5, pp. 483-488, doi:10.1038/ngeo1496.
- Cobb, J.T. and Principe, J.C. [2011]. *Seabed segmentation in synthetic aperture sonar images*. In proceedings of SPIE Defense and Security Symposium, Vol. 8017.
- Cobb, J.T.; Slatton, K.C.; and Dobeck, G.J. [2010]. *A parametric model for characterizing seabed textures in synthetic aperture sonar images*. IEEE Journal of Oceanic Engineering, Vol. 35, No. 2, pp. 250-266.
- Cook, D. [2007]. *Synthetic aperture sonar motion estimation and compensation*. M.Sc. thesis, School of Electrical and Computer Engineering, Georgia Institute of Technology, Atlanta, GA, USA.
- Devey, C.W.; Jamieson, J.W.; Petersen, S.; Yeo, I.A.; Walter, M.; Buss, A.; Collins, J.; Koehler, J.; Palgan, D.; and Vishiti, A. [2013]. *Predicting the location of extinct massive sulfide deposits on the Atlantic seafloor*. American Geophysical Union Fall Meeting abstract, 2013AGUFMOS43A1867D.
- The Economist [2014]. *Deep secrets*. The Economist Newspaper Limited, Sept. 6.
- Ellefmo, S. [2014]. *Marine minerals and ocean mining potential in the North*

- Atlantic*. Underwater Mining Institute Presentation, Lisbon, Portugal.
- Ferri, G.; Jakuba, M.V.; and Yoerger, D.R. [2010]. *A novel trigger-based method for hydrothermal vents prospecting using an autonomous underwater robot*. *Autonomous Robots*, Vol. 29, No. 1, pp. 67-83. doi:10.1007/s10514-010-9187-y.
- Fundis, A.T.; Soule, S.A.; Fornari, D.J.; and Perfit, M.R. [2010]. *Paving the seafloor: volcanic emplacement processes during the 2005-2006 eruptions at the fast spreading East Pacific Rise, 9°50'N*. *Geochemistry, Geophysics, Geosystems*, Vol. 11, No. 8, Q08024, doi:10.1029/2010GC003058.
- German, C.R.; Yoerger, D.R.; Jakuba, M.V.; Shank, T.M.; Langmuir, C.H.; and Nakamura, K. [2008]. *Hydrothermal exploration with the Autonomous Benthic Explorer*. *Deep-Sea Research Part 1: Oceanographic Research Papers*, Vol. 55, No. 2, pp 203-219.
- Ghiglia, D.C. and Pritt, M.D. [1998]. *Two-dimensional phase unwrapping: theory, algorithms, and software*. Wiley and Sons, Inc.
- Jakowatz, J.C.V.; Wahl, D.E.; Eichel, P.H.; Ghiglia, D.C.; and Thompson, P.A. [1996]. *Spotlight-mode synthetic aperture radar: a signal processing approach*. Dordrecht, The Netherlands: Kluwer.
- Hagen, P.E. and Hansen, R.E. [2011]. *Synthetic aperture sonar on AUV: making the right trade-offs*. *Journal of Ocean Technology*, Vol. 6, No. 2, pp. 17-22.
- Hansen, R.E. [2011]. *Introduction to synthetic aperture sonar*. Sonar Systems, ISBN: 978-953-307-345-3, InTech, September. Retrieved from: www.intechopen.com/books/sonarsystems/introduction-to-synthetic-aperture-sonar.
- Hansen, R.E.; Callow, H.J.; Sæbø, T.O.; and Synnes, S.A.V. [2011]. *Challenges in seafloor imaging and mapping with synthetic aperture sonar*. *IEEE Transactions on Geoscience and Remote Sensing*, Vol. 49, No. 10, pp. 3677-3687.
- Hansen, R.E. [2013]. *Synthetic aperture sonar technology review*. *Marine Technology Society Journal, The State of Technology in 2013*, Vol. 47, No. 5.
- Hanssen, R.F. [2001]. *Radar interferometry: data interpretation and error analysis*. Dordrecht, The Netherlands: Kluwer Academic Publishers.
- Hawkins, D.W. [1996]. *Synthetic aperture imaging algorithms: with application to wide bandwidth sonar*. PhD dissertation, Department of Electrical and Electronic Engineering, University of Canterbury, Christchurch, New Zealand.
- Hayes, M.P. and Gough, P.T. [2009]. *Synthetic aperture sonar: a review of current status*. *IEEE Journal of Oceanic Engineering*, Vol. 34, No. 3, pp. 207-224.
- Heyes, C. [2002]. *Offshore diamond mining*. Marcon International Inc. Retrieved from: www.marcon.com/marcon2c.cfm?SectionListsID=85&PageID=281.
- Kelley, D.S.; Karson, J.A.; Früh-Green, G.L.; Yoerger, D.R.; Shank, T.M.; Butterfield, D.A.; and Sylva, S.P. [2005]. *A serpentinite-hosted ecosystem: the Lost City hydrothermal field*. *Science*, Vol. 307, pp. 1428-1434. doi:10.1126/science.1102556.
- Kelley, D.S. and Shank, T.M. [2010]. *Hydrothermal systems: A decade of discovery in slow spreading environments*. *Geophysical Monograph Series*, Vol. 188, pp. 369-407. doi:10.1029/2010GM000945.

- Krasnov, S.G.; Cherkashev, G.A.; and Stepanova, T.V. [1995]. *Detailed geographical studies of hydrothermal fields in the North Atlantic*. Geological Society, London, Special Publications, Vol. 87, pp. 43-64.
- Lipton, I. [2012]. *Mineral resource estimate: Solwara Project, Bismarck Sea, Papua New Guinea*. Nautilus Minerals and Golder Associates Technical Report. Report no. 107631040-003-R-Rev 1.
- Lurton, X. [2010]. *An introduction to underwater acoustics: principles and applications*. Second edition, Springer Praxis Publishing.
- Massonnet, D. and Souyris, J. [2008]. *Imaging with synthetic aperture radar*. EFPL Press.
- Mitchell, N.C.; Allerton, S.; and Escartin, J. [1998]. *Sedimentation on young ocean floor at the Mid-Atlantic Ridge, 29°N*. Marine Geology, Vol. 148, pp.1-8.
- Nautilus Minerals Inc. [2014]. *Nautilus enters into vessel charter*. Investor Press Release, Vancouver, BC.
- Oliver, C. and Quegan, S. [1998]. *Understanding synthetic aperture radar images*. Artech House, Inc.
- Pedersen, R.B.; Thorseth, I.H.; Hellevang, B.; Schultz, A.; Taylor, P.; Knudsen, H.P.; and Steinsbu, B.O. [2005]. *Two vent fields discovered at the ultraslow spreading Arctic Ridge System*. American Geophysical Union Fall Meeting 2005, abstract #OS21C-01. Retrieved from: <http://adsabs.harvard.edu/abs/2005AGUFMOS21C..01P>.
- Pedersen, R.B.; Thorseth, I.H.; Lilley, M.D.; Fruh-Green, G.I.; Barriga, F.; Rapp, H.T.; Baumberger, T.; Flesland, K.; and Jørgensen, S.L. [2009]. *Discovery of the Loki's Castle Vent field at the ultra-slow spreading Arctic Mid-Ocean Ridge*. *Geochimica et Cosmochimica Acta*. 73: A1008-A1008.
- Pedersen, R.B.; Rapp, H.T.; Thorseth, I.H.; Lilley, M.D.; Barriga, F.; Baumberger, T.; Flesland, K.; Fonseca, R.; Fruh-Green, G.L.; and Jørgensen, S.L. [2010A]. *Discovery of a black smoker vent field and vent fauna at the Arctic Mid-Ocean Ridge*. Nature Communications, doi:10.1038/ncomms1124.
- Pedersen, R.B.; Thorseth, I.H.; Nygård, T.E.; Lilley, M.D.; and Kelley, D.S. [2010B]. *Hydrothermal activity at the Arctic Mid-Ocean Ridges*. In Diversity of Hydrothermal Systems on Slow Spreading Ocean Ridges, Geophysical Monograph Series 188. doi:10.1029/2008GM000783.
- Sæbø, T.O.; Synnes, S.A.V.; and Hansen, R.E. [2013]. *Wideband interferometry in synthetic aperture sonar*. IEEE Transactions in Geoscience and Remote Sensing, Vol. 51, No. 8, pp. 4450-4459.
- Singh, H.; Roman, C.; Pizarro, O.; Eustice, R.; and Can, A. [2007]. *Towards high-resolution imaging from underwater vehicles*. International Journal of Robotics Research, Vol. 26, No. 1, doi:10.1177/0278364907074473.
- Sternlicht, D.D.; Fernandez, J.E.; and Marston, T.M. [2012]. *Detecting, classifying mines with synthetic aperture acoustic tomography: advances in SAS create detailed images in challenging environments*. Sea Technology Magazine, November.
- Szitkar, F.; Dymant, J.; Choi, Y.; and Fouquet, Y. [2014A]. *What causes low magnetization at basalt-hosted hydrothermal sites? Insights from inactive site Krasnov (MAR 16°38'N)*. *Geochemistry, Geophysics,*

- Geosystems, Vol. 15, pp. 1441-1451, doi:10.1002/2014GC005284.
- Szitkar, F.; Dymant, J.; Choi, Y.; Fouquet, Y.; and Horen, H. [2014B]. *The magnetic signature of ultramafic-hosted hydrothermal sites*. *Geology*, Vol. 42, No. 8, doi:10.1130/G35729.1.
- Thorseth, I.H.; Pedersen, R.B.; Kruber, C.; and Kosler, J. [2007]. *Low-temperature hydrothermal deposits at the 71N vent fields at the Arctic Mid-Ocean Ridge: architecture, microtextures, and geochemistry*. American Geophysical Union Fall Meeting, abstract OS43A-0996. Retrieved from: <http://adsabs.harvard.edu/abs/2007AGUFMOS43A0996T>.
- Tivey, M.A. and Johnson, H.P. [2002]. *Crustal magnetization reveals subsurface structure of Juan de Fuca Ridge hydrothermal vent fields*. *Geology*, Vol. 30, pp. 979-982, November. doi:10.1130/0091-7613.
- Tivey, M.A.; Johnson, H.P.; Salmi, M.S.; and Hutnak, M. [2014]. *High-resolution near-bottom vector magnetic anomalies over Raven Hydrothermal Field, Endeavour Segment, Juan de Fuca Ridge*. *Journal of Geophysical Research, Solid Earth*, Vol. 119, No. 10, pp. 7389-7403, doi:10.1002/2014JB011223.
- Veirs, S.R.; McDuff, R.E.; Lilley, M.D.; and Delaney, J.R. [1999]. *Locating hydrothermal vents by detecting buoyant, advected plumes*. *Journal of Geophysical Research*, Vol. 104, No. B12, pp. 29239-29247, doi:10.1029/1999JB900291.
- Whiffen, G. [2014]. *C.B.S. company part of Arctic mission that found Franklin expedition wreck*. *The Telegram*. Retrieved from: www.thetelegram.com/News/Local/2014-09-12/article-3866550/C.B.S.-company-part-of-Arctic-mission-that-found-Franklin-expedition-wreck/1.
- Yoerger, D.R.; Jakuba, M.; Bradley, A.; and Bingham, B. [2007]. *Techniques for deep sea near bottom survey using an autonomous underwater vehicle*. *International Journal of Robotics Research*, Vol. 26, No. 1. doi:10.1177/0278364907073773.
- Øvreås, L.; Johannesen, T.; Jørgensen, S.L.; Thorseth, I.H.; and Pedersen, R.B. [2007]. *Diversity of microorganisms associated with low temperature iron deposits at the 71°N Hydrothermal Vent Field along the Arctic Mid-Ocean Ridge*. American Geophysical Union Fall Meeting, abstract OS43A-0992. Retrieved from: <http://adsabs.harvard.edu/abs/2007AGUFMOS43A0992O>.